Study of the influence of physical nonlinearities of spherical caps made by Elastomeric Materials

P.F.S. Oliveira[1], R. M. Soares[1]

[1] *School of Civil and Environmental Engineering, University of Goiás*
University Avenue, Plot Area 1488,74605-220, Goiás/Goiânia, Brazil
patriciafernanda@discente.ufg.br, renatasoares@ufg.br

Abstract. In this study, the behavior of a shell with a spherical cap geometry was investigated, where the boundary condition was established by crimping the base circumference. The material properties ranged from linear elastic to hyperelastic, with validation conducted using elastic theory. Deformation-displacement relationships were determined using Novozhilov nonlinear shell theory adapted for spherical shells. Hooke's Law was employed for linear elastic materials, while the Neo-Hookean model represented the nonlinear elastomeric material. The Rayleigh-Ritz numerical method applied to the Potential Energy Functional was used to derive the energy-based equation, with trigonometric functions employed for circumferential direction approximation and Legendre polynomials for the meridional direction. Results showed natural frequency values consistent with literature, as well as nonlinear behavior observed through frequency-amplitude relationships. Static behavior under uniformly distributed dead load was also validated against existing literature.

Keywords: spherical shells, elastomeric materials, novozhilov, neo-hookean, legendre polynomial.

1   Introduction

Shells are prevalent in engineering and are utilized across various sectors including aerospace, aeronautics, mechanics, shipbuilding, civil engineering, and even biotechnology. In construction, they are predominantly employed in roofing applications, particularly in the roofs of large structures such as the domes of historic cathedrals.

This paper focuses on spherical shells belonging to the category of shells of revolution, characterized by having a rotational axis, often referred to as a generatrix, as demonstrated by Brasil [1]. Dias [2] studied the contribution made in the formulations by authors like Reissner – Meissner, Hildebrand, Sander's e Flügge-Lur'e – Byrne. And authors like Alhazza [3], Du et.al [4] and Shen et. al [5] based their research on classical theories.

When discussing the physical attributes of an element, the type of material comprising it defines its properties. For instance, elastomeric materials, particularly hyperelastics, possess the ability to rapidly alter and regain the initial dimensions of the object under stress. This behavior stems from the fact that elastomers constitute a group of rubbery polymers with chemical and physical cross-links.

Hoss [6] elaborates on the evolution of the constitutive relations of hyperelastic materials, which is marked by the development of various physical-mathematical models categorized based on genealogy and chronology, including names like Mooney, Treolar, Rivlin, Sanders, Odgen and Yeoh.

This study investigates the behavior of spherical caps constructed from elastic and hyperelastic materials, aiming to compare the outcomes of these materials to delineate differences in linear and nonlinear analyses. Novozhilov's theory was employed to characterize the geometry of the cap. For the materials, Hooke's theory was applied to elastic materials, and the Neo-Hookean theory was utilized for hyperelastic materials.

2   Mathematical Formulations

The spherical cap's geometry was derived from Larriccio and Pellicano [7], who defined parameters such as radius R, radius of the circular base a, height s, half-opening angle ϕ_b, and thickness h, as illustrated in Fig. 1. The curvilinear coordinate system adopted was (O, ϕ, θ), where O denotes the origin, and ϕ and θ represent the meridional and circumferential coordinates, respectively.

Additionally, was introduced three displacement fields to characterize the motion of a general point P on the surface. Considered $u(\phi,\theta,t)$, $v(\phi,\theta,t)$, and $w(\phi,\theta,t)$, as the displacements in the meridional, circumferential, and radial directions, respectively, with t denoting the temporal variable.
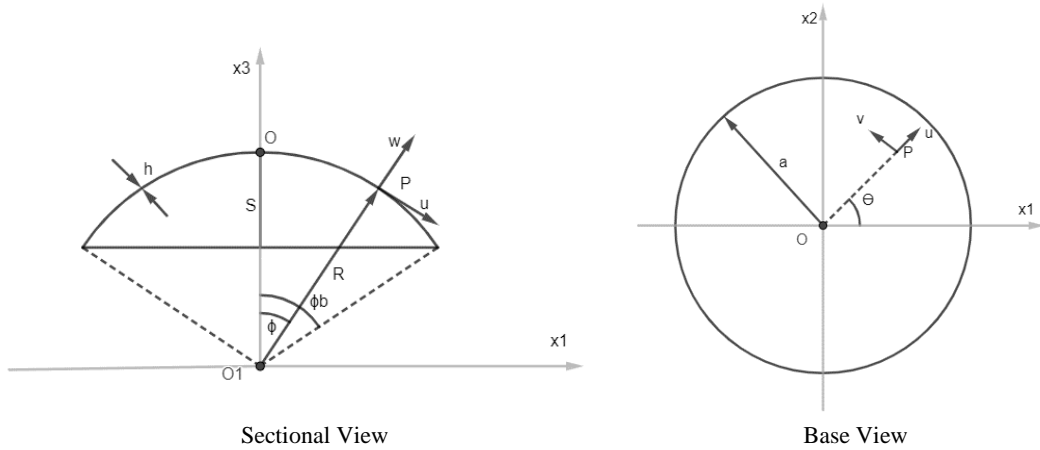
Figure 1. Spherical Cap Coordinate System (Larriccio and Pellicano [7])

2.1   Novozhilov Theory applied to Spherical Caps

Novozhilov's classical theory for doubly thin curved shells is based on the Love-Kirchhoff assumptions, in which the linearity approximation is considered. Also is considered the Vlasov definition approximation about the curvature, that was applies to a spherical cap with a small elevation s compared to the radius of the base circle a (where the ratio s/a must be less than 1/5). Therefore, the Lamé coefficients can be written by the eq. (1).

$$A_1 = R \, , \, A_2 = R \cdot \phi_b \cdot \eta \text{ e } A_3 = 1 \, . \tag{1}$$

The non-dimensional meridional coordinate, derived from the relation $\eta=\phi/\phi_b$, is utilized. To avoid singularity problems, the initial value of η_0 adopted is 0.00125.

The components in the curvilinear coordinate system for the spherical cap can be written according to the eq. (2) until eq. (7).

$$e_{11} = \frac{1}{A_1} \cdot \frac{\partial u}{\phi_b \partial \eta} + \frac{w}{R} \, . \tag{2}$$

$$e_{12} = \frac{1}{A_2} \cdot \frac{\partial u}{\partial \theta} - \frac{1}{A_1 \cdot A_2} \cdot \frac{\partial A_2}{\phi_b \cdot \partial \eta} \cdot v \, . \tag{3}$$

$$e_{13} = -\frac{u}{R} + \frac{1}{A_1} \cdot \frac{\partial w}{\phi_b \cdot \partial \eta} \, . \tag{4}$$

$$e_{21} = \frac{1}{A_1} \cdot \frac{\partial v}{\phi_b \cdot \partial \eta} \, . \tag{5}$$

$$e_{22} = \frac{1}{A_1 \cdot A_2} \cdot \frac{\partial A_2}{\phi_b \cdot \partial \eta} \cdot u + \frac{1}{A_2} \cdot \frac{\partial v}{\partial \theta} + \frac{w}{R} . \tag{6}$$

$$e_{23} = -\frac{v}{R} + \frac{1}{A_2} \cdot \frac{\partial w}{\partial \theta} . \tag{7}$$

The deformations at an arbitrary point on the shell are given by eq. (8) until eq. (10).

$$\hat{\varepsilon}_\eta = \varepsilon_\eta + z \cdot k_\eta . \tag{8}$$

$$\hat{\varepsilon}_\theta = \varepsilon_\theta + z \cdot k_\theta . \tag{9}$$

$$\hat{\gamma}_{\eta\theta} = \gamma_{\eta\theta} + z \cdot k_{\eta\theta} . \tag{10}$$

And the components of the deformations and curvature changes are shown in eq. (11) until eq. (16).

$$\varepsilon_\eta = e_{11} + \frac{1}{2} \cdot \left(e_{11}^2 + e_{12}^2 + e_{13}^2 \right) . \tag{11}$$

$$\varepsilon_\theta = e_{22} + \frac{1}{2} \cdot \left(e_{21}^2 + e_{22}^2 + e_{23}^2 \right) . \tag{12}$$

$$\gamma_{\eta\theta} = e_{12} + e_{21} + e_{11} \cdot e_{21} + e_{12} \cdot e_{22} + e_{13} \cdot e_{23} . \tag{13}$$

$$k_\eta = -\frac{1}{A_1} \cdot \frac{\partial e_{13}}{\phi_b \cdot \partial \eta} + \frac{e_{11} + e_{22}}{R} . \tag{14}$$

$$k_\theta = -\frac{1}{A_1 \cdot A_2} \cdot \frac{\partial A_2}{\phi_b \cdot \partial \eta} \cdot e_{13} - \frac{1}{A_2} \cdot \frac{\partial e_{23}}{\partial \theta} + \frac{e_{11} + e_{22}}{R} . \tag{15}$$

$$k_{\eta\theta} = -\frac{1}{A_2} \cdot \frac{\partial e_{13}}{\partial \theta} - \frac{1}{A_1} \cdot \frac{\partial e_{23}}{\phi_b \cdot \partial \eta} + \frac{1}{A_1 \cdot A_2} \cdot \frac{\partial A_2}{\phi_b \cdot \partial \eta} \cdot e_{23} . \tag{16}$$

2.2   Potential Energy Functional and Work of External Forces

The Energy Functional, eq. (17), is formulated as a combination of the internal strain energy U_S eq. (18), kinetic energy T_S, eq. (19), and Work of External Forces W_S, eq. (20), when static behavior is considered.

$$L = T_s + U_s - W_s . \tag{17}$$

$$U_s = \iiint_V (W) dV . \tag{18}$$

$$T_s = \frac{1}{2} \cdot \rho_s \cdot h \int_{\eta 0}^1 \int_0^{2\cdot\pi} \left(\dot{u}^2 + \dot{v}^2 + \dot{w}^2 \right) A_1 \cdot A_2 \cdot \phi_b d\theta d\eta . \tag{19}$$

$$W_S = \int_{\eta 0}^1 \int_0^{2\cdot\pi} qz \cdot w \cdot A_1 \cdot A_2 \cdot \phi_b d\theta d\eta . \tag{20}$$

where, S denotes the area of the average surface, which, in this context, refers to the average surface of the shell, and V represents the volume. Additionally, the variable W signifies the strain energy density, ρ_S denotes the density of the material, and qz represents the distributed dead load applied to the external surface.

2.3 The internal Strain Energy

The internal strain energy U_S is defined by the strain energy density, W, that is described by the material used. For elastic materials, W is written from Hooke's law and, after doing mathematical manipulation, U_S can be write as eq. (21).

$$U_s = \frac{1}{2} \cdot \frac{E \cdot h}{1-v^2} \int_{\eta 0}^{1} \int_{0}^{2 \cdot \pi} \left(\varepsilon_\eta^2 + \varepsilon_\theta^2 + 2 \cdot v \cdot \varepsilon_\eta \cdot \varepsilon_\theta + \frac{1-v}{2} \cdot \gamma_{\eta\theta}^2 \right) A_1 \cdot A_2 \cdot \phi_b d\theta d\eta$$
$$+ \frac{1}{2} \cdot \frac{E \cdot h^3}{12 \cdot (1-v^2)} \cdot \int_{\eta 0}^{1} \int_{0}^{2 \cdot \pi} \left(k_\eta^2 + k_\theta^2 + 2 \cdot v \cdot k_\eta \cdot k_\theta + \frac{1-v}{2} \cdot k_{\eta\theta}^2 \right) \cdot A_1 \cdot A_2 \cdot \phi_b d\theta d\eta \qquad (21)$$

The strain energy density, W, for non-linear material, the Neo-Hookean model is described by eq. (22).

$$W = \frac{\mu_1}{2} \cdot (I_1 - 3). \qquad (22)$$

where I_1 is the first deformation invariant shown in eq. (23); and μ_1, the material parameter, can be described as a function of the Modulus of Elasticity, E, by eq. (24) when use $v = 0.5$.

$$I_1 = 2 \cdot \left(\hat{\varepsilon}_\eta + \hat{\varepsilon}_\theta + \hat{\varepsilon}_R \right) + 3. \qquad (23)$$

$$\mu_1 = \frac{E}{4 \cdot (1+v)} = \frac{E}{6}. \qquad (24)$$

The expression for the transverse strain can be written as a series around zero and composed of the components of the other strains, like eq. (25).

$$\hat{\varepsilon}_R = \frac{1}{2 \cdot \left(\left(2\hat{\varepsilon}_\eta + 1 \right) \cdot \left(2\hat{\varepsilon}_\theta + 1 \right) - \left(\hat{\gamma}_{\eta\theta} \right)^2 \right)} - \frac{1}{2}. \qquad (25)$$

2.4 Rayleigh-Ritz Method

The approximated functions of the displacements used on Rayleigh-Ritz Method was shown on eq. (26) until eq. (28).

$$u(\eta,\theta,t) = U(\eta,\theta) \cdot f(t) \xrightarrow[where]{} U(\eta,\theta) = \sum_{m=0}^{Mu} \sum_{n=0}^{N} U_{m,n} \cdot P_m^*(\eta) \cdot \cos(n \cdot \theta). \qquad (26)$$

$$v(\eta,\theta,t) = V(\eta,\theta) \cdot f(t) \xrightarrow[where]{} V(\eta,\theta) = \sum_{m=0}^{Mv} V_{m,0} \cdot P_m^*(\eta) + \sum_{m=0}^{Mv} \sum_{n=1}^{N} V_{m,n} \cdot P_m^*(\eta) \cdot \sin(n \cdot \theta). \qquad (27)$$

$$w(\eta,\theta,t) = W(\eta,\theta) \cdot f(t) \xrightarrow[where]{} W(\eta,\theta) = \sum_{m=0}^{Mw} \sum_{n=0}^{N} W_{m,n} \cdot P_m^*(\eta) \cdot \cos(n \cdot \theta). \qquad (28)$$

In this case, the shape functions are trigonometric and are already written as a function of the coordinate system used. In addition, the nodal coefficients ($U_{m,n}$, $V_{m,n}$, $W_{m,n}$) are written as a function of m and n, i.e. the half-waves generated in the two directions (meridional and circumferential).

The Legendre polynomial $P_m^*(\eta) = P_m^*(2\eta-1)$, m is the m-th Legendre polynomial of the first displaced type in the domain $\eta \in [0,1]$. The function $f(t) = \cos(\omega t)$ was used to dynamic behavior. After that, applied the derivation of Functional.

3 Numerical Results

The geometric characteristic of the spherical cap is $R = 0.8$ m; h/R (h) = 1/300 (0.00267 m); $a = 0.152$ m; $s = 0.0147$ m; $\phi_b = 11° = 0.191986$ radians. The physical properties considered include $E = 1247060.2$ Pa; $\rho_s = 1380$ kg/m³, $v = 0.5$, with crimping applied throughout its base. The degrees of freedom (dof) adopted was 14.

3.1 Natural Frequencies in Free Vibration

Comparing the natural frequency responses found for the elastic and hyperelastic cases, the elastic frequency value is considerably lower than the hyperelastic frequency, in the order of 0.016%. The values are exposed on Tab. 1.

Table 1. Comparison of Natural Frequencies (elastic and hyperelastic materials)

Elastic ω (rad/s)	Hyperelastic ω (rad/s)
51.7381	51.7465

The values of the natural frequencies suggest similarity in the vibration modes obtained by changing the type of material, which is best ascertained by analyzing the behavior of the displacements (u, v and w) normalized by the maximum value, as shown Fig 2.
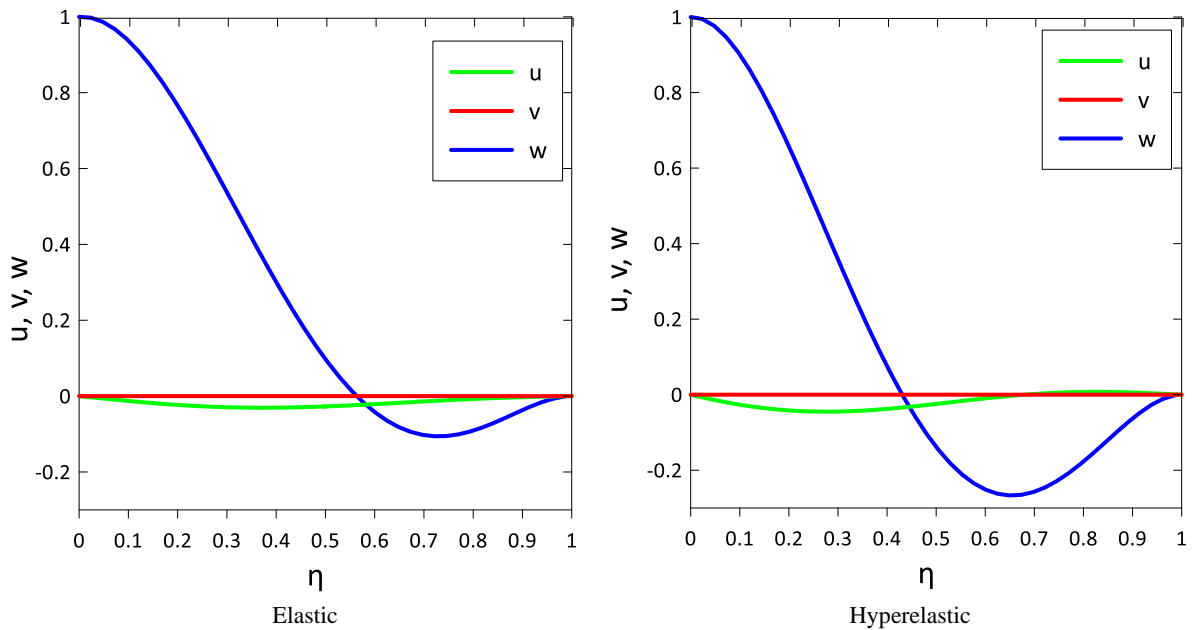
Figure 2. Displacements by Vibration modes

In both cases the transverse displacement is the biggest one. And the hyperelastic mode revel that are bigger half-waves than the elastic mode.

3.2 Frequency – amplitude (non-linear dynamics)

The frequency-amplitude relation was applied to the center coordinates of the spherical cap ($\theta=0°$, $R=0.8$ e $\eta=0$), and the amplitude chosen was the nodal coefficient $W_{2,0}$ normalized by the thickness h. The curve behavior was exposed on Fig. 3.

Analyzing the curves revealed a consistent non-linear pattern in the stiffness gain across both elastic and hyperelastic scenarios. While there's minimal discrepancy between the two cases, it's evident that the hyperelastic material exhibits a higher amplitude.

Elastic and Hyperelastic   Hyperelastic (extended)
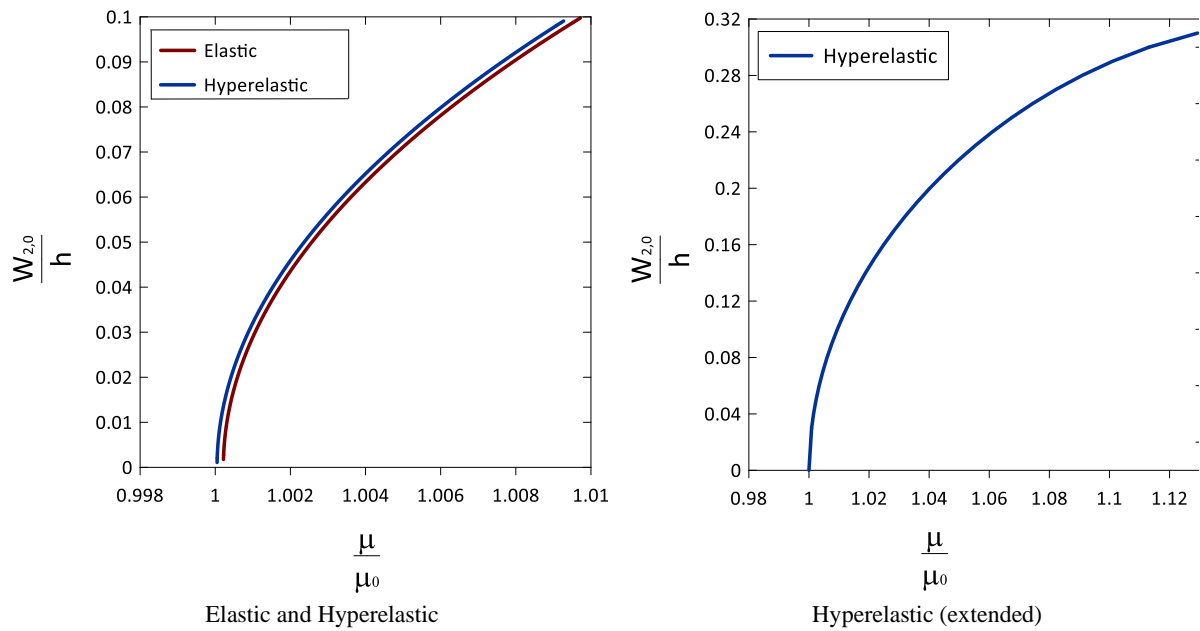
Figure 3. Frequency - Amplitude (Elastic x Hyperelastic materials)

3.3 Static Analysis

The equilibrium paths for the elastic and hyperelastic cases are depicted in Fig. 4. It's evident that as the load rises, the displacement values similarly increase in both scenarios. Moreover, the elastic material exhibits considerably smaller displacements compared to the hyperelastic case under identical loading conditions, after the section where it experiences greater loading gain than displacement. This suggest that is only the beginning of the hyperelastic curve, that will increase more displacements after that.

Elastic and Hyperelastic   Hyperelastic (extended)
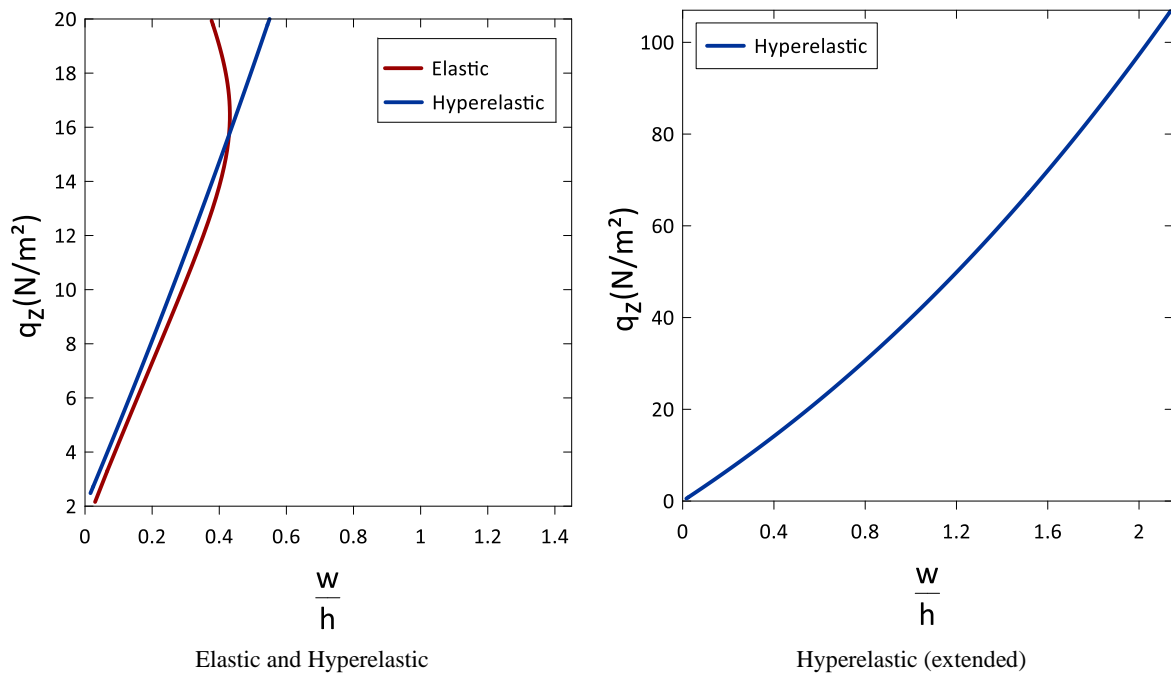
Figure 4. Load *versus* displacement relations (Elastic x Hyperelastic materials)

4   Conclusions

In this investigation, we delve into the nonlinear static and dynamic characteristics of a thin spherical cap employing an energy-based methodology. Material properties are delineated through the utilization of Hooke's Law for the elastic regime and the neo-Hookean model for the hyperelastic domain.

Upon examining free vibration, the hyperelastic cap exhibits little higher natural frequencies compared to the elastic counterpart. Additionally, a subtle difference in mode shapes emerges between the two materials, with the hyperelastic material demonstrating larger half-waves than elastic. Furthermore, the nonlinear tendencies observed in free vibration reveal that both materials experience stiffness gain, but the hyperelastic material demonstrates slightly greater stiffness compared to the elastic material.

In terms of equilibrium paths, it is observed that the elastic material undergoes smaller displacements relative to the hyperelastic material after a section that present more gain of load than displacement.

These divergences in behavior underscores the propensity of hyperelastic materials to exhibit augmented displacements and higher vibrations.

Authorship statement. The authors hereby confirm that they are the sole liable persons responsible for the authorship of this work, and that all material that has been herein included as part of the present paper is either the property (and authorship) of the authors or has the permission of the owners to be included here.

References

[1] R. M. L. R. F Brasil. Sheets, plates and shells in aerospace engineering. *Blucher*, 1a ed. 164 p. São Paulo, 2020.
[2] A. Dias. Stress Analysis in Semi-Thick Revolution Shells using the Finite Differences Method. Advisor: Raul Guenther. 1981. *Dissertation (Master's)*. Mechanical Engineering Course. Federal University of Santa Catarina. Santa Catarina, Brazil, 1981. Accessed. Apr 16, 2023. Available at:
https://repositorio.ufsc.br/xmlui/bitstream/handle/123456789/76740/180788.pdf?sequence=1&isAllowed=y.
[3] K. A. Alhazza. Nonlinear Vibrations of Doubly Curved Cross-Ply Shallow Shells. Supervisor: Dr. Ali H. Nayfeh. 2002. *Dissertation (Doctoral Degree)*. Mechanical Engineering.
[4] Y. Du. et al. Free vibration of spherical cap subjected to various boundary conditions. *Advances in Mechanical Engineering*, 2019.
[5] Y. Shen. et al. Predicting the Type of Nonlinearity of Shallow Spherical Shells: Comparison of Direct Normal Form with Modal Derivatives. *Advances in Nonlinear Dynamics, Proceedings of the Second International Nonlinear Dynamics Conference (NODYCON 2021)*. Vol. 1 (pp.361-371).
[6] L. Hoss. Hyperelastic Constitutive Models for Incompressible Elastomers: Adjustment, Performance Comparison, and Proposal of a New Model. Advisor: Prof. Dr. Rogério José Marezak. *Dissertation (Master's)*. Rio Grande do Sul, 2009. Accessed on Apr 17, 2023. Available at https://lume.ufrgs.br/handle/10183/16310.
[7] G. Larriccio and F. Pellicano. Nonlinear Dynamics and Stability of Shallow Spherical Caps Under Pressure Loading. *Journal of Computational and Nonlinear Dynamics*, 2021.